JOURNAL OF GEOPHYSICAL RESEARCH, VOL. 101, NO. A12, PAGES 27,187–27,198, DECEMBER 1, 1996

Modeling the global magnetic field of the large-scale Birkeland current systems

Nikolai A. Tsyganenko

Hughes STX Corporation, Laboratory for Extraterrestrial Physics, NASA Goddard Space Flight Center Greenbelt, Maryland

David P. Stern

Laboratory for Extraterrestrial Physics, NASA Goddard Space Flight Center, Greenbelt, Maryland

Abstract. Quantitative models are developed for representing the global distribution of the average magnetic field produced by the region 1 and 2 Birkeland current systems. The problem is solved in four following steps: (1) constructing a realistic tilt-dependent model of the Birkeland current sheets, based on the formalism of Euler potentials, (2) numerically computing their field at a large number of points within the modeling region, (3) finding a best-fit analytical approximation for that field, and (4) adding a current-free shielding field which confines the Birkeland field within the model magnetopause. At low altitudes the model field-aligned currents reach the ionosphere along eccentric ovals, which fit the observed region 1 and 2 zones of Iijima and Potemra, and they continue there as horizontal currents. At larger distances the nightside region 1 currents map to the plasma sheet boundary layer and are then diverted toward the tail flanks, while currents in the dawn-dusk and dayside sectors connect directly to the higher-latitude magnetopause. The region 2 current closes azimuthally near the equator, forming a spread-out partial ring current system. The described approach allows a great flexibility in the geometry of the Birkeland currents, making it feasible to infer their properties from spacecraft data.

1. Introduction

Birkeland current systems, discovered by *Zmuda and Armstrong* [1974] and statistically studied by *Iijima and Potemra* [1976] 2 decades ago, have not been included until now in data-based models of the magnetosphere, although there exists strong evidence for their significant effect upon the configuration of the Earth's distant magnetic field. Though earlier empirical models [*Mead and Fairfield*, 1975; *Tsyganenko*, 1987, 1989] did not contain explicit modules for the field of Birkeland currents, they indicated a persistent equatorward shift of the dayside polar cusps with growing level of disturbance, which could not be entirely attributed to the effects of an increased tail and/or ring current. Later studies [*Tsyganenko et al.*, 1993; *Tsyganenko and Sibeck*, 1994; *Donovan*, 1993] confirmed that both the dayside and nightside effects of the field-aligned currents were comparable with the contributions from other sources.

Several attempts were made previously [*Tsyganenko*, 1988, 1991, 1993; *Stern*, 1993; *Donovan*, 1993] to quantitatively describe the effects of Birkeland current systems. However, none of those models proved to be realistic enough and/or computationally feasible to be calibrated against spacecraft data. The purpose of this work is to describe a new model of the Birkeland field, which will be included as a separate component in an advanced model of the Earth's magnetosphere.

Paper number 96JA02735.
0148-0227/96/96JA-02735$09.00

2. Region 1 Birkeland Current System

One of the principal difficulties with Birkeland currents, not found in other current systems, is the lack of information on their actual global configuration. While there exists a relatively clear picture of the spatial distribution of these currents at low altitudes (400−1000 km), little is as yet known on where they flow and close at larger geocentric distances. The existing concepts are based mainly on indirect evidence, such as the correlations of the low-altitude currents with the solar wind parameters [*Bythrow and Potemra*, 1983], statistical studies of the magnetic shear in the plasma sheet boundary layer [*Candidi et al.*, 1990; *Tsyganenko et al.*, 1993], model mappings [e.g., *Tsyganenko and Sibeck*, 1994], and theoretical arguments [e.g., *Stern*, 1983; *Troshichev*, 1982].

Another potentially valuable source of information is emerging now, as computer simulations of the magnetosphere are becoming more realistic. For instance, a recent study by *Tanaka* [1995] traces the flow of region 1 currents from the ionosphere to the magnetopause. It is quite interesting that, according to the simulation results, the region 1 Birkeland currents significantly divert from the magnetic field lines for $R \geq 6 - 8\,R_E$, in other words, the condition $\vec{\mathbf{j}} \parallel \vec{\mathbf{B}}$ breaks down in the distant magnetosphere. The same result was recently obtained in the magnetohydrodynamic simulations by *Janhunen et al.* [1996].

According to the above results, the dayside part of the region 1 oval most likely maps to the vicinity of the boundary layer adjacent to the magnetopause, while at the nightside the currents map to the plasma sheet boundary layer and, after turning around and heading toward the tail flanks, may connect there to the solar wind.

The geometry of the Birkeland currents is also expected to depend on the tilt angle of the Earth's dipole: at ionospheric altitudes the location of both region 1 and 2 ovals is approximately fixed in solar-magnetic coordinates, while in the outer magnetosphere the driving effect of the solar wind causes the plasma sheet, which is closely associated with the nightside Birkeland currents, to gradually line up with the Sun-Earth direction.

The model of the region 1 system should be sufficiently flexible to reproduce the aforementioned features, so that when fitting the model to large sets of spacecraft measurements, the data could determine the actual average configuration of the currents.

We model the field of the Birkeland currents in the following four steps.

1. Specify the electric current flow and intensity in terms of suitable Euler potentials, imposing a desired geometry on the model current distribution.

2. Numerically compute the magnetic field of the current system described above at many points within the modeling region by means of Biot-Savart integration.

3. Use the resulting set of magnetic field vectors as a "database" to which simple analytical representations of the model field are fitted.

4. Derive and add to the specified field a current-free "shielding" field, confining the Birkeland field within the model magnetopause.

The model of the Birkeland current field thus obtained forms a separate module, which can be included in the quantitative representation of the net magnetospheric field and fitted to a large set of spacecraft data. The results of such a global modeling study are relegated to a separate paper, while in this work we concentrate on details of the Birkeland field model itself.

2.1. Specifying the Region 1 Current Sheet

The region 1 current model satisfies the following requirements.

1. At low altitudes the currents flow along dipolar field lines, and the current sheet maps in the ionosphere along a near-circular closed line, approximating the observed region 1 zone of *Iijima and Potemra* [1976]. The intensity of the region 1 current in the model varies with the magnetic local time (MLT), so that the inflowing and outflowing currents peak near 0900 and 1500 MLT, respectively, in agreement with the statistical result of *Iijima and Potemra* [1976]. However, in this idealized model we assume that the spatial distribution of the currents is symmetric with respect to the noon-midnight meridian plane.

2. At larger distances the shape of the current layer reflects the distortion of the background magnetic field, stretched tailward on the nightside. In the tail, the Birkeland currents map to the outer layers of the plasma sheet [e.g. *Tsyganenko et al.*, 1993] and are gradually diverted to the tail flanks. On the dayside the field-aligned currents extend to higher latitudes and reach the magnetopause in the vicinity of the polar cusps.

3. At low altitudes the current sheet position is tied to the observed Iijima-Potemra oval and is therefore approximately fixed in solar-magnetic coordinates, following the orientation of the Earth's dipole. At larger distances on the nightside, the Birkeland current sheet follows the stretched magnetotail field lines and warps in response to changing geodipole tilt, together with the tail plasma sheet.

The magnetic field of the Birkeland current is curl-free outside the current sheet and is therefore represented there by analytical scalar potentials having different forms in the inner (low-latitude) and outer (high-latitude) regions with respect to the current sheet. Actually, the current occupies a layer of finite thickness, and a simple interpolation procedure smoothly models the field in the transition region, spreading out the electric current density across the layer.

Because we seek to specify the flow lines of electric current, and because the electric current density $\vec{\mathbf{j}}$ satisfies $\nabla \cdot \vec{\mathbf{j}} = 0$, it is convenient to represent it in terms of Euler potentials:

$$\vec{\mathbf{j}} = \nabla\xi_1 \times \nabla\chi_1 \tag{1}$$

Using the Euler potentials is especially convenient because they allow one to label points of space and thus define their relative position with respect to the current sheet.

Formally, the representation (1) yields a three-dimensional distribution of the volume current density, so that $\vec{\mathbf{j}} \neq \mathbf{0}$ at any point of space. However, we use (1) only for constructing the current flow lines with footpoints lying on the Iijima-Potemra oval, with the purpose of using them as "wires" in the Biot-Savart integration, and we then assume that there is no current outside of the sheet.

The Euler potentials ξ_1 and χ_1 are defined so that close to the high-latitude ionosphere they reduce to functions of the dipole Euler potentials $\alpha_d = \sin^2\theta/r$ and ϕ, which guarantees that the lines of $\nabla\xi_1 \times \nabla\chi_1$ automatically follow dipolar magnetic field lines at low altitudes. However, at larger distances one must take into account both the nondipolar deformation of distant field lines and the fact that electric current flow lines in the tail break away from magnetic field lines as they approach the equator. A suitable form is

$$\alpha' = \left\{ r^n \left[(\sin\theta)^{-2n} - 1 \right] + 1 \right\}^{-1/n} \tag{2}$$

which reduces to the dipolar Euler potential α_d in the limit of $\theta \to 0$, while at sufficiently large distances the surfaces of constant α' extend in the radial direction and asymptotically approach the equatorial plane, so that their shape in meridional planes resembles the stretched field lines in the tail plasma sheet.

It is convenient to use $\Theta_0 = \Theta_0(r, \theta)$ in place of α', defined by $\sin^2\Theta_0 = \alpha'$, so that a line with a given value of Θ_0, e.g., $\Theta_0(r, \theta) = \Theta^\star$, reaches Earth's surface at colatitude $\Theta^\star$.

The parameter n in (2) can take arbitrary values; however, for $n = 3$, the lines of constant Θ_0 most closely match the shape of the model magnetospheric field lines [e.g., *Tsyganenko*, 1995] with the footpoint colatitudes in the range

$10° \leq \Theta_0 \leq 20°$, corresponding to the location of the region 1 oval. Figure 1 shows a family of lines of constant Θ_0 given by (2) with $n = 3$, providing the coordinate system for constructing the model region 1 current sheet.

Actually, the surface followed by the lines of $\vec{\mathbf{j}}$ should reach Earth at a variable colatitude $\Theta_i(\phi)$, approximating the region 1 oval found by Iijima and Potemra [1976]. We therefore define

$$\xi_1(r, \theta, \phi) = \Theta_0(r, \theta) - \Theta_i(\phi) \tag{3}$$

and assume that the current sheet follows the surface $\xi_1 = 0$. This makes the electric current flow lines with footpoints at longitude ϕ follow near-Earth dipole field lines starting at colatitude $\Theta_i(\phi)$. The form chosen was a simple approximation

$$\Theta_i{}^{(N)} = \Theta_{\text{noon}} + \Delta\Theta \sin^2 \frac{\phi}{2} \tag{4}$$

$$\Theta_i{}^{(S)} = \pi - \Theta_i{}^{(N)} \tag{5}$$

where the superscripts (N) and (S) refer to the Northern and Southern hemispheres, respectively. The numerical values of the parameters $\Theta_{\text{noon}} = 12°$ and $\Delta\Theta = 8°$ were specified in accordance with the average shape and position of the region 1 oval obtained by *Iijima and Potemra* [1976].

Adopting the potential ξ_1 in the form (3) guarantees that the current flow lines remain on the surface $\xi_1(r, \theta, \phi) = 0$ having the necessary properties. To obtain the desired shape of the current flow lines on that surface, we have to specify the second Euler potential in (1), χ_1. It is convenient to represent it as

$$\chi_1 = G_1(r)\, f_1(\phi) \tag{6}$$

separating the dependence on the radial distance r and the longitude ϕ into two independent factors. Near Earth the factor G_1 should be nearly constant, which makes the azimuthal component of $\vec{\mathbf{j}}$ in (1) tend to zero for small r. Since ξ_1 in that region is approximately a function of the dipole Euler potential α_d and χ_1 is a function only of ϕ, then, by (1), $\vec{\mathbf{j}}$ automatically follows dipole field lines at low altitudes. In the present version of the model, we assumed

$$G_1(r) = \left[(r/r_0)^\kappa + 1\right]^{-1} \tag{7}$$

with $r_0 = 30R_E$ and $\kappa = 10$.

The second factor, $f_1(\phi)$, controls the local time distribution of both azimuthal and field-aligned components of the current, so that $j_\phi \propto f_1$ and $j_\parallel \propto f_1'$. The following form was assumed in this model:

$$f_1(\phi) = A\left[b^4\left(\frac{\phi^2 - \pi^2}{\phi^2 + b^2}\right)^2 - \epsilon\pi^4\right] \tag{8}$$

where the parameter b controls the longitudinal position of the peaks of the field-aligned current density at ionospheric altitude; for small values of b, the peak current occurs near noon, while larger values shift it closer to the dawn-dusk meridian. The parameter ϵ controls the relative amount of the current closing at large distances across the noon and midnight meridian planes: if $\epsilon = 1$, then $j_\phi = 0$ at $\phi = 0$ and j_ϕ peaks at $\phi = \pi$, i.e. all current flow lines are diverted to the nightside, and there is no closure across the noon meridian plane. In the opposite case, $\epsilon = 0$, there is no closure across the midnight meridian, so that the current flow lines with the ionospheric footpoints on the night side are diverted away from the midnight meridian plane and close on the dayside. We assume the nightside currents to enter and exit the magnetosphere at the tail flanks, rather than being generated inside the plasma sheet. Therefore the factor $f_1(\phi)$ should equal zero at the midnight meridian, and hence we choose $\epsilon = 0$. The factor A in (8) is a normalization constant.

The electric current model specified by (1)–(8) is quite simple and flexible, allowing a variety of possible configurations. Using Euler potentials is of crucial importance, since it allows one to easily determine the position of a given point with respect to the electric current sheet.

Figures 2 show the shape of the current flow lines in the model (only lines of the northern hemisphere are displayed). Figure 2a shows the lines in their whole extent, while in Figure 2b the lines were traced only inside the magnetosphere, until they hit the model magnetopause.

Near the Earth's surface the currents flow along dipolar field lines and close in the ionosphere across the polar cap as circular segments oriented in the dawn-dusk direction.

As shown in the plots, on the nightside the current flow lines first map to the plasma sheet boundary layer and then are diverted to the flanks, in agreement with the expected geometry of Birkeland currents. In the dawn-dusk and dayside sectors the currents map to the higher-latitude magnetopause, in line with their proposed origin on open field lines, as is discussed above.

It is important to note that the family of electric current flow lines, shown in Figure 2a, does not represent the final

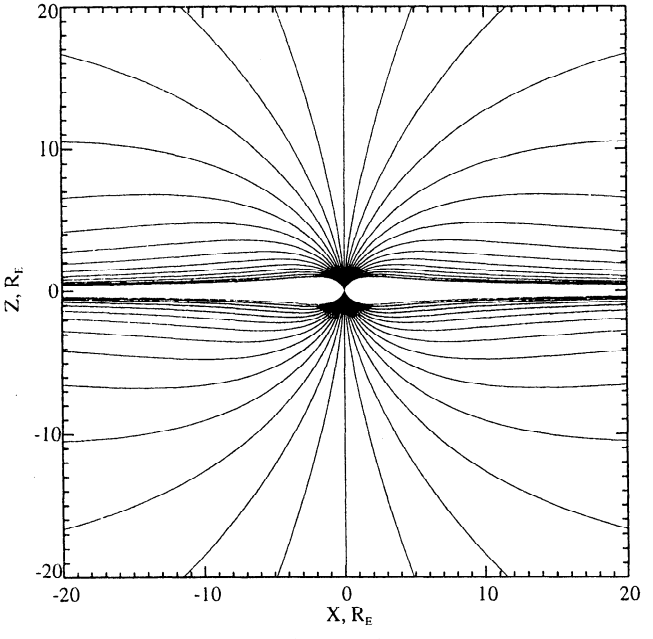

Figure 1. Coordinate lines of constant $\Theta_0(r, \theta) = \arcsin\left(\alpha'^{1/2}\right)$, given by (2) with $n = 3$ and providing a coordinate system for modeling the region 1 currents.

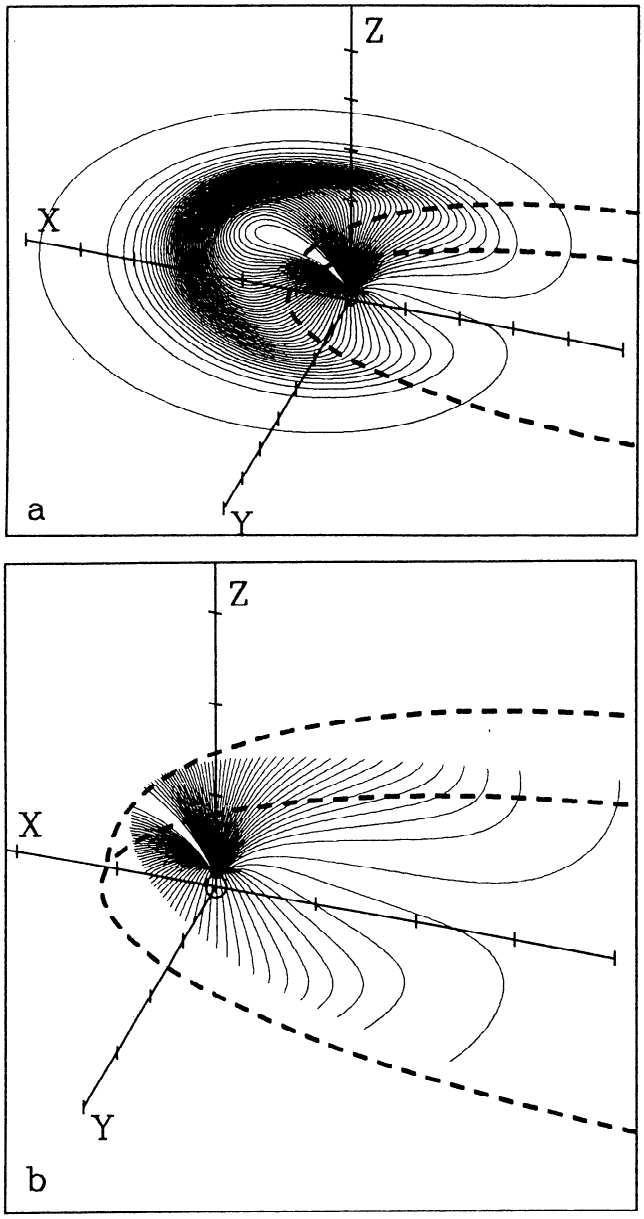

Figure 2. Three-dimensional view of the model region 1 electric current flow lines, defined by equations (1)–(8). (a) The current sheet in its entirety, with the flow lines starting from the ionosphere on the dusk side, crossing the noon meridian plane sunward from Earth, then arriving back to the ionosphere on the dawn side and closing via the polar cap. (b) The same flow lines, but only inside the magnetosphere. As is discussed in the text, the addition of the shielding field is equivalent to closing the currents in Figure 2b via the magnetopause surface currents (not shown here). The position of the model magnetopause (cross sections in the equatorial and noon-midnight meridian planes) is shown by dashed lines.

configuration of the model current; rather, it corresponds to the unshielded field of the Region 1 system. As is discussed in more detail in section 2.4, the existence of a magnetopause leads to a major modification of both the magnetic field and global pattern of the electric current. The assumption of full shielding (i.e., $B_n = 0$) uniquely determines that modification, no matter how the currents close outside the magnetosphere. Because the exact mode of closure makes no difference (and is in any case not known), it will be assumed that the circuit closes by surface currents lying on the model magnetopause.

2.2. Effects of the Geodipole Tilt

The dipole tilt effects were modeled by introducing a tilt-dependent warping of coordinates in the modeling region. More specifically, the Cartesian coordinates (X, Y, Z), entering implicitly in (1), were replaced by $(X^\star, Y, Z^\star)$, where

$$X^\star = X\cos\Psi^\star - Z\sin\Psi^\star$$
$$Z^\star = X\sin\Psi^\star + Z\cos\Psi^\star \tag{9}$$

The angle $\Psi^\star = \Psi^\star(r, \Psi)$, specifying rotation around the Y axis, is a function of the dipole tilt angle Ψ and of the radial distance r, so that at the Earth's surface $\Psi^\star$ equals Ψ, but it decreases gradually with increasing geocentric distance, and falls off to zero in the distant magnetosphere. The specific functional form for $\Psi^\star$ used in this model and providing the desired warping reads as follows

$$\sin\Psi^\star = \frac{\sin\Psi}{r}\times \frac{\sqrt{(R_H+r)^2+\Delta R^2}-\sqrt{(R_H-r)^2+\Delta R^2}}{\sqrt{(R_H+1)^2+\Delta R^2}-\sqrt{(R_H-1)^2+\Delta R^2}} \tag{10}$$

where the parameter R_H is the geodipole's "radius of influence" and ΔR is the scale thickness of the transition layer between the dipole- and the solar-wind-dominated regions. The values $R_H = 9R_E$ and $\Delta R = 3R_E$ were chosen in the current version of the model. Figure 3 displays the family of lines of constant coordinates $X^\star$ and $Z^\star$, illustrating the

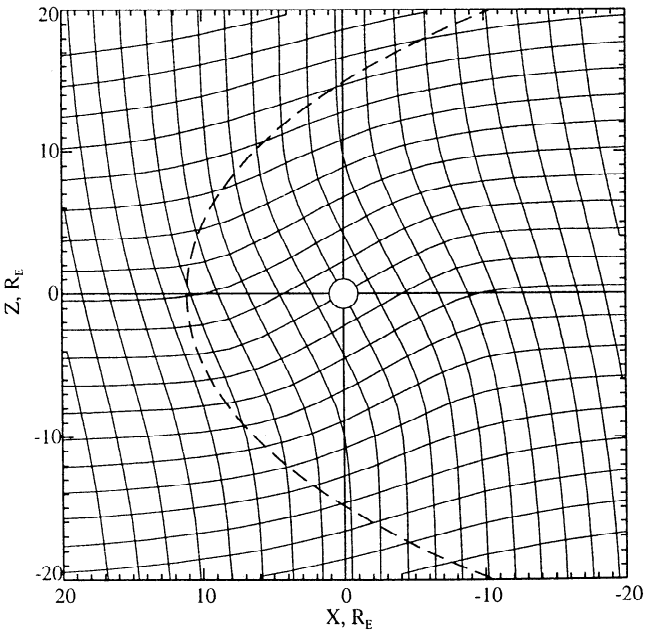

Figure 3. The tilt-dependent coordinate system, defined by equations (9)–(10). The warped coordinate lines in the noon-midnight meridian correspond to the dipole tilt angle of $\Psi = 30°$.

warping effect: at low altitudes the starred coordinates are close to the solar-magnetic ones, while at larger distances the lines of constant Z^* become aligned parallel to the solar wind flow, resembling in shape the warped current sheet of the magnetotail. Note that a similar transformation was suggested by *Hedgecock and Thomas* [1975] for representing the HEOS data in the curvilinear "geocentric magnctospheric equatorial" (GME) coordinates.

Using the starred coordinates (9) in equation (1) leads to the desired deformation of the Birkeland current sheet for $\Psi \neq 0$ and expands the representation (1) for the electric currents by Euler potentials to the full range of tilt angles.

We will discuss the dipole tilt effects further in the next section.

2.3. Approximating the Region 1 Field in the Inner and Outer Modeling Domains, and in the Transition Region Between Them

The magnetic field produced by the model Region 1 Birkeland currents was obtained as follows. The whole space between the ionosphere and the model magnetosphere was divided into five domains, parametrized by the Euler potential $\xi_1 = \Theta_0 - \Theta_i$: domain I, the northern high-latitude region $\Theta_0 < \Theta_i^{(N)} - \delta\Theta_0$; domain II, the southern high-latitude region $\Theta_0 > \Theta_i^{(S)} + \delta\Theta_0$; domain III, the low-latitude region $\Theta_i^{(N)} + \delta\Theta_0 < \Theta_0 < \Theta_i^{(S)} - \delta\Theta_0$; domain IV, the northern transition region $\Theta_i^{(N)} - \delta\Theta_0 \leq \Theta_0 < \Theta_i^{(N)} + \delta\Theta_0$; and domain V, the southern transition region $\Theta_i^{(S)} - \delta\Theta_0 \leq \Theta_0 < \Theta_i^{(S)} + \delta\Theta_0$.

Figure 4 shows the configuration of the region 1 current sheet in the noon-midnight meridian plane, displayed together with the magnetic field lines in the data-based magnetospheric model for average conditions: solar wind pressure $p = 2$ nPa, $Dst = -10$ nT, $AE = 250$ nT, IMF $B_y = 0$, and a small southward $B_z = -2$ nT, which gives rise to a nonzero normal component across the model magnetopause, as shown in the plot [*Tsyganenko and Stern*, 1995].

At the nightside, the transition region can be associated with the plasma sheet boundary layer, and its half-thickness is defined by the parameter $\delta\Theta_0$, which corresponds to the latitudinal half-thickness of the Iijima-Potemra oval at the ionospheric altitude. In the present model, this parameter was set equal to $\delta\Theta_0 = 2°$.

The Biot-Savart integration was performed for two sets of points, comprising 14,725 points in the outer (high-latitude) domains I and II and 9,862 points in the inner (low-latitude) domain III, covering the spatial region $1R_E \leq R \leq 60R_E$ and including seven values of the dipole tilt angle in the range $0° \leq \Psi \leq 35°$ (because of symmetry, it suffices to consider positive values only). The above numbers of points were chosen in order to keep a reasonable compromise between the requirements of sufficient accuracy and computational limitations. The integration was done by approximating the volume current distribution as a collection of current sheets, each of which was further approximated by a collection of wires. The advantage of "wires" over volume or surface integrals is that the continuity of current is automatically guaranteed; the disadvantage is a "graininess" of the magnetic field within the region occupied by the currents themselves, which requires taking special measures (described in more detail in subsection 3.2.1).

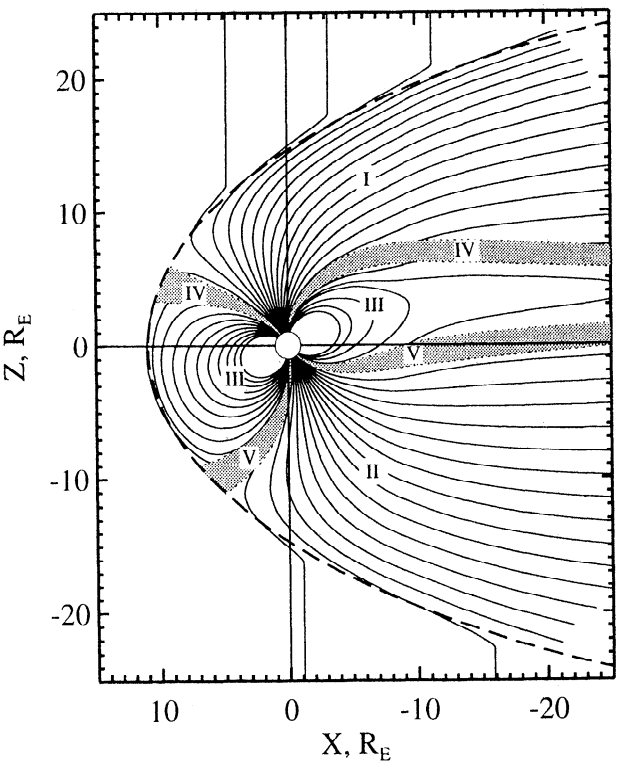

Figure 4. Location of the model region 1 current sheet (shaded area) with respect to the background magnetospheric magnetic field lines, plotted for average magnetospheric conditions, as given by a data-based model with a small southward interplanetary magnetic field [*Tsyganenko and Stern*, 1995].

Arrays of Biot-Savart field vectors thus obtained were then used for finding best-fit approximations for the curl-free magnetic field in domains I–III. The field in the plasma sheet boundary layer domains IV and V, containing the model current sheets, was computed by interpolating between the values on the boundary, which spread out the thin current sheets into a wider diffuse layers.

The success of such an approach depends critically on the quality of the analytical approximation of the fields in the current-free regions. This is why the choice of the approximating functions, described in the next subsection, is of paramount importance.

2.3.1. Approximating the field in the low-latitude domain. The curl-free magnetic field in domain III can be represented by a variety of harmonic functions. After many trial runs with different kinds of potential fields, we chose a combination of conical harmonics with a set of image dipoles located outside of the modeling region.

The conical harmonics [*Tsyganenko*, 1991] are curl-free vector potentials, derived by separating variables in the equation $\nabla \times \nabla \times \vec{\mathbf{A}} = \mathbf{0}$ and assuming that the potential $\vec{\mathbf{A}}$ is purely radial (and hence that the corresponding magnetic field is purely toroidal). The result is a set of harmonics

$$\vec{\mathbf{A}} = (\vec{\mathbf{r}}/r)(\tan^m \frac{\theta}{2} + \cot^m \frac{\theta}{2}) \sin m\phi \,. \qquad (11)$$

Note that the same curl-free magnetic fields can be obtained by assuming a scalar potential in the form $U(r, \theta, \phi) = f(\theta, \phi)/r^n$ and solving Laplace's equation for $n = 0$. In the case $n = 1$, the angular dependence in the scalar potential remains the same as in (12), but the field has also a nonzero radial component, and in the case $n \geq 2$ the potential is expressed in standard spherical harmonics.

In this work, we used the conical harmonics (equation (11)), appropriate for $n = 0$, retaining the first five terms in the expansion in m for A_r.

The corresponding magnetic field is inversely proportional to r, establishing the behavior of the model field at small altitudes. To improve the fitting, we added to that field the contribution from a set of 36 dipoles placed on four planes parallel to the solar-magnetic equatorial plane, at $Z_{SM} = \pm 4R_E$ and $Z_{SM} = \pm 20R_E$. Another set of 10 dipoles was placed on the Z_{SM} axis. Simultaneous fitting of the moments of the dipoles and the amplitudes of the conical harmonics to the Biot-Savart field yielded an rms fit better than 3% of the rms field over the whole modeling region and in the range $-35^\circ \leq \Psi \leq 35^\circ$ for the dipole tilt angles.

2.3.2. Approximating the field in the high-latitude domains. Several sets of harmonic expansions were tried for fitting the Biot-Savart field in the high-latitude regions. In the end we chose a combination of image dipoles with a set of three current loops, located near the equatorial plane. The current loops have a circular shape, which ensures a sufficiently smooth spatial variation of the model field and at the same time allows computationally effective code. The moments of the dipoles as well as the current loop positions and strengths were fitted by least squares to the Biot-Savart field, also yielding an rms accuracy of about 3%.

2.3.3. Approximating the field in the transition region and the interpolation procedure. By construction, the approximations used here for the magnetic fields in the low- and high-latitude regions are divergence- and curl-free and closely match the Biot-Savart field, whose normal component B_n is continuous across the current sheet, while the tangential one exhibits a jump, proportional to the surface current density. Therefore one can expect that a smooth interpolation of the magnetic field vector across the transition layer between the two regions will spread out the initially thin current sheet over a finite thickness and approximately conserve the property $\nabla \cdot \vec{\mathbf{B}} = 0$ inside the current sheet.

Each of the five domains in Figure 4 corresponds to a range of the Euler potential ξ_1 in (1), and each of the separating surfaces has a specific value of ξ_1. Given a point in space, one thus easily finds by calculating its ξ_1 to which region it belongs. In case the point is inside one of the transition regions, its value of ξ_1 allows one to find straddling points (X_1, Y_1, Z_1) and (X_2, Y_2, Z_2) on the bounding surfaces enclosing the transition, and then one can perform linear interpolation between those points.

2.4. Derivation of the Shielding Field

As was noted above, the electric current system shown in Figure 2a extends outside the magnetopause, in a way which is obviously nonrealistic, and its magnetic field extends continuously across the magnetopause as well. Assuming a closed magnetosphere in which B_n on the magnetopause is zero (an assumption that can later be modified by adding a suitable interconnection field [*Toffoletto and Hill*, 1989]), we add a current-free field $\vec{\mathbf{B}} = -\nabla U$ which cancels any nonzero B_n and thus enforces the "full-shielding" boundary condition, confining the field of Birkeland currents inside the magnetopause. After that the field outside the magnetosphere can be set equal to zero and, as was discussed by *Sotirelis et al.* [1994] with regard to the tail current system, such a procedure is equivalent to redirecting the currents outside the magnetosphere, making them flow on the boundary and thereby close the internal part of the current system. The actual geometry of the currents outside the magnetopause may differ, but because perfect shielding was assumed, the field on the inside is not affected by whatever happens outside, so that one may assume the currents close on the magnetopause.

The shielding field for the Birkeland current systems can be easily found by an approach used for other principal sources of the magnetospheric field [*Schulz and McNab*, 1987; *Tsyganenko*, 1995]. Namely, we choose appropriate flexible potential fields with a sufficient number of degrees of freedom (e.g., harmonic expansions for a scalar potential, or a combination of various current sheets) and fit their parameters by least squares, to achieve a minimal rms $\langle B_n^2 \rangle$ on the magnetopause.

In this model we used a superposition of rectangular harmonics for the shielding scalar potential, similar to those used for the tail field shielding in the model of *Tsyganenko* [1995]:

$$U = \sum_{i,k=1}^{N} (a_{ik} + b_{ik} \cos\Psi) \exp\left[\sqrt{\frac{1}{p_i^2} + \frac{1}{p_k^2}}\, X\right] \times \cos\frac{Y}{p_i} \sin\frac{Z}{p_k} + \sum_{i,k=1}^{N} (c_{ik} \sin\Psi + d_{ik} \sin 3\Psi) \times \exp\left[\sqrt{\frac{1}{q_i^2} + \frac{1}{q_k^2}}\, X\right] \cos\frac{Y}{q_i} \cos\frac{Z}{q_k} \qquad (12)$$

The potential (12) proved to be quite effective in shielding the Birkeland field, and with $N = 5$ it reduced the rms residual $\langle B_n^2 \rangle^{1/2}$ at the magnetopause to about 1% of that of the unshielded field.

3. Modeling the Region 2 Birkeland Current System

The field of the region 2 currents was modeled by essentially the same method. However, the geometry of the region 2 currents is different in several aspects from that of the region 1 system, as follows:

1. The entire circuit of the region 2 currents is believed to be contained inside the magnetosphere and to be closed by a partial ring current on the nightside. Therefore different forms of the Euler potentials should be used instead of functions (3) and (6).

2. The region 2 currents are observed at lower latitudes, where the field is closer to that of a dipole. Hence one may as an approximation assume that the field-aligned currents and the associated partial ring current are rigidly tied to the Earth's dipole, so that their configuration in the solar-magnetic coordinates is not affected by changes of the dipole tilt angle, in contrast to the region 1 system.

3. The MLT distribution of the region 2 field-aligned currents at ionospheric altitude differs from that of region 1 in that the maxima of its current density are shifted to the nightside from the dawn-dusk meridian, rather than being on its dayside.

4. The greatest difficulty with the region 2 current system is the relatively wide radial extension of its partial ring current in the low-latitude near-equatorial region, which means that the simple method of representing the magnetic field components in this area by interpolating between their boundary values would lead to significant inaccuracies in the electric current and large deviations of $\nabla \cdot \vec{\mathbf{B}}$ from zero.

The rest of this section discusses in more detail the way the region 2 model addresses the above points.

3.1. Representing the Region 2 Electric Current

As was noted in section 2.1, the representation (1) for the region 1 currents was not intended to model the spread-out distribution of the volume current density across the current sheet. Rather, it was used only for constructing a thin current sheet by tracing the current flow lines from the region 1 oval in the ionosphere. The case of the region 2 system is somewhat different: as was mentioned above, the thin-sheet approximation is too crude there. The Euler potential representation similar to (1) is also used for $\vec{\mathbf{j}}$, but it must be modified to represent a thick current layer, in which the current density is smoothly distributed within a relatively large range of the coordinate ξ and is zero outside it.

The easiest way to do that is to multiply the vector product $\nabla\xi \times \nabla\chi$ by a scalar "form factor" $p(\xi)$, providing a smooth distribution of the electric current density which is bell-shaped in the vicinity of the region 2 surface and which vanishes outside the current layer. According to this, we assumed the region 2 current density to have the form

$$\vec{\mathbf{j}} = (\nabla\xi_2 \times \nabla\chi_2) \cdot p(\xi_2) \tag{13}$$

It is easy to check that the above modification does not violate the continuity of current density, so that (13) satisfies $\nabla \cdot \vec{\mathbf{j}} = 0$ with any function $p(\xi_2)$. In this model, a simple single-peak function was adopted as the form factor for the current density:

$$p(\xi) = \begin{cases} \cos^2\left(\dfrac{\pi\xi}{2\Delta\xi_2}\right) & \text{for } |\xi| \le \Delta\xi_2 \\ 0 & \text{for } |\xi| > \Delta\xi_2 \end{cases} \tag{14}$$

where $\Delta\xi_2$ is the halfthickness of the current sheet in the ξ space. In the present model, we assumed $\Delta\xi_2 = 0.035$, so that a region 2 zone with a latitudinal width of 5° in the ionosphere maps to a relatively wide region $-10 \le X \le -5R_E$ in the nightside equatorial magnetosphere.

The first Euler potential for the region 2 current system was chosen as

$$\xi_2 = \alpha_d(\tilde{r}, \tilde{\theta}) - \alpha_d(1, \Theta_i(\tilde{\phi})) \tag{15}$$

where the function $\alpha_d(\tilde{r}, \tilde{\theta})$ was a stretched modification [*Stern*, 1987] of the dipole Euler potential $\alpha_d(r, \theta) = \sin^2\theta/r$, with stretched coordinates denoted by tildes. The purpose of the stretch transformation was to make the shape of the region 2 current sheet closer to the average observed shape of the magnetic field lines with footpoints on the centerline of the Iijima-Potemra region 2 oval. The function Θ_i in (15) has a form similar to that for the region 1 model (4),

$$\Theta_i = \Theta_{\text{noon}} + \Delta\Theta \sin^2\frac{\tilde{\phi}}{2} \tag{16}$$

but with different values of the parameters: $\Theta_{\text{noon}} = 21°$ and $\Delta\Theta = 5.5°$, so that the region 2 oval is located at lower latitudes, and its day-night asymmetry is smaller than that of region 1.

We adopted a three-dimensional Cartesian stretch transformation, in which perturbation terms were added to all three coordinates, so that x, y, and z in the purely dipolar Euler potentials were replaced by

$$\begin{aligned} f &= x + f_1(x, y, z) \\ g &= y + g_1(x, y, z) \\ h &= x + h_1(x, y, z) \end{aligned} \tag{17}$$

respectively, where

$$\begin{aligned} f_1 &= \left[a_1 + a_2\frac{x}{r} + a_3\frac{x^2}{r^2} + a_4\frac{y^2}{r^2} + a_5\frac{z^2}{r^2}\right]q(r) \\ g_1 &= \left[b_1\frac{y}{r} + b_2\frac{xy}{r^2}\right]q(r) \\ h_1 &= \left[c_1\frac{z}{r} + c_2\frac{xz}{r^2}\right]q(r) \end{aligned} \tag{18}$$

The coefficients of expansions (18) were found by least squares, from the requirement that the stretched field vectors in the vicinity of the region 2 current system provide the closest directional fit to a data-based model field [*Tsyganenko*, 1995; *Tsyganenko and Stern*, 1995] for average conditions. Note also that the expansions (18) contain a smooth function $q(r)$, which gradually increases with r, at the same time q and q' are zero inside the sphere $r = R_0 \approx 1.2R_E$, so that the dipolar coordinates remain intact near the ionosphere.

Figure 5 shows the magnetospheric magnetic field configuration, chosen for fitting the parameters of the stretch transformation (17)–(18), similar to that in Figure 4. The shaded area in the figure corresponds to the location of the distributed partial ring current and associated region 2 Birkeland current, whose boundaries are given by the surfaces $\xi_2 = \pm\Delta\xi_2$. As can be seen in the plot, these boundaries do not exactly match the shape of the model field magnetic lines because of the inevitable inaccuracies of representing the model field by a simple stretching of dipolar lines.

The second Euler potential for the region 2 system, χ_2, was assumed to have the form

$$\chi_2 = G_2(\gamma)\, f_2(\phi) \tag{19}$$

in which, as in (6), we also expressed the dependence on the longitude by a separate factor $f_2(\phi)$. However, the quasi-dipolar geometry of the region 2 and the partial ring current system suggested the use of the coordinate $\gamma = \cos\theta/r^2$ as the argument in G_2 [*Stern*, 1993; *Tsyganenko*, 1993], instead of the radius r, as in (6)–(7). More specifically, we chose

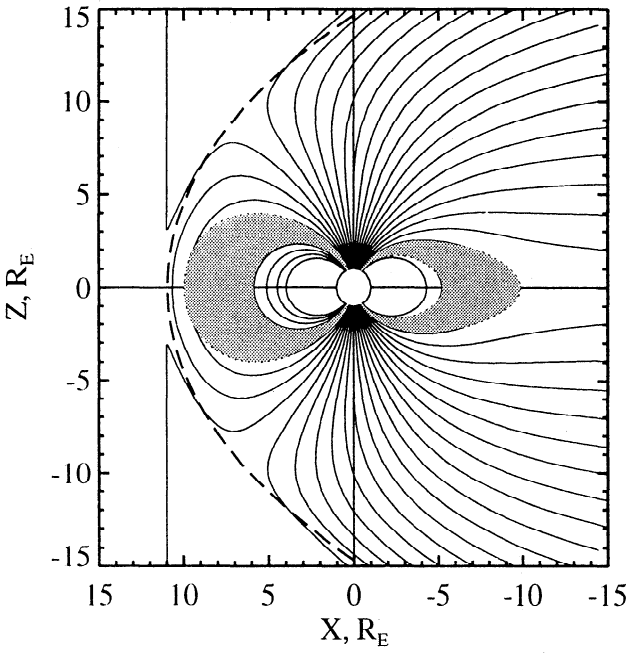

Figure 5. Location of the region 2 currents (shaded area) with respect to the same magnetospheric field configuration as in Figure 4. The day-night asymmetry of the region 2 system was fitted to that of the background field by using the stretch transformation of the dipolar field, given by equations (17)–(18).

$$G_2(\gamma) = \frac{\gamma}{\sqrt{\gamma^2 + \gamma_0^2}} \tag{20}$$

where the value $\gamma_0 = 0.006$ provided the closest fit to the latitudinal distribution of the partial ring current density obtained by *Tsyganenko* [1993] as the exact solution of the continuity equation for an azimuthally asymmetric distribution of isotropic plasma in a purely dipolar magnetic field.

The longitudinal factor $f_2(\phi)$ was assumed to have a form similar to $f_1(\phi)$ in the region 1 model, given by (8). The shift of the peak of the current of region 2 to the nightside, noted earlier, was achieved by rotating the distribution (8) by 180° around the Z_{SM} axis, so that $\phi \Rightarrow \phi - \pi$. The parameter ϵ in this case was also set equal zero. All region 2 field-aligned currents are assumed to close across the midnight meridian in this model, as shown in Figure 6 (and implied by physical arguments).

3.2. Approximating the Region 2 Magnetic Field

To approximate the Biot-Savart field in the inner and outer curl-free regions outside of the region 2 current sheet shown in Figure 5, we used potential fields in the same form as for the region 1 current system. As was mentioned at the beginning of this section, we reduced the geodipole tilt effects to simple rigid rotation of the entire region 2 system around the Y axis, so that the fitting was made in solar-magnetic coordinates, assuming $\Psi = 0$. Owing to the absence of terms containing Ψ, the approximating forms here were much simpler.

However, as was already said above, when modeling the region 2 system, one encounters the problem of representing the field inside the thick region with spread-out currents. The large spatial extent of this region, combined with a complex curved geometry of the current flow lines, makes it unfeasible to employ the interpolation method used for approximating the region 1 field. We adopted a different approach, desribed in the following subsection.

3.2.1. The model field inside the region 2 current sheet. The magnetic field inside the current sheet is not curl-free and hence cannot be approximated by the gradient of a scalar potential. In principle, one could try to find appropriate vector potentials, either by fitting a model potential $\vec{\mathbf{A}}(\vec{\mathbf{r}})$ to the one obtained from the electric current by Biot-Savart integration or by fitting the vector $\nabla \times \nabla \times \vec{\mathbf{A}}$ to the current density given by equation (13). However, neither of those two approaches yielded satisfactory results, so it was finally decided to abandon vector potentials. Instead, the single thick current sheet was replaced by a set of parallel sheets filling the transition region, their field $\vec{\mathbf{B}}_S$ was derived by Biot-Savart integration, and separate best fit analytical approximations were found for three components of $\vec{\mathbf{B}}_S$. Although this approach does not automatically guarantee that the field is divergence-free (as do vector potentials), the approximate condition $\nabla \cdot \vec{\mathbf{B}} \approx \mathbf{0}$ should still hold with a sufficient accuracy, provided the fit to the Biot-Savart field $\vec{\mathbf{B}}_S$ is close enough, because $\vec{\mathbf{B}}_S$ is divergence-free by construction.

To numerically derive the field inside the current layer between the surfaces $\xi_2 = -\Delta\xi_2$ and $\xi_2 = \Delta\xi_2$, nine additional surfaces $\xi_2 = k\Delta\xi_2$ were inserted in the space between them, with $k = -0.8, -0.6, ..., 0.6, 0.8$. Each of the 11 surfaces was then assumed to carry a fraction of the current commensurate with (14), and the current on each surface, in its turn, was shared by 99 evenly spaced "wires," obtained by numerically tracing flow lines of the electric current vector (13) like those shown in Figure 6, closed across the polar cap in the ionosphere. Magnetic fields from each wire were

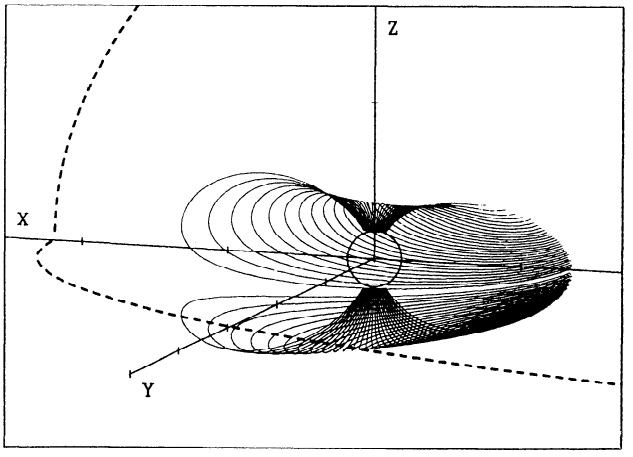

Figure 6. The configuration of the region 2 electric current flow displayed in three dimensions. Only one sheet of current flow lines is shown here for the sake of visual clarity; a set of 11 such sheets, located within a wide layer (the shaded area in Figure 5), was used for calculating the magnetic field. The position of the model magnetopause (the dusk portion of the equatorial section and the northward noon meridian section) is shown by dashed lines.

derived by Biot-Savart integration and summed. Altogether the Biot-Savart field $\vec{\mathbf{B}}_S$ was obtained for 2759 points.

The derivation of the Biot-Savart integral at a point inside the region of closely spaced current sheets required special care because contributions from the sections of the wires closest to the point involve small denominators, which can greatly increase the numerical inaccuracy. In order to reduce that problem, we derived the integral at points located exactly halfway between the neighbor sheets, and the segments of the wires closest to the derivation point were omitted from the summation.

Given a set of magnetic field vectors $\vec{\mathbf{B}}_S$ inside the region of currents, the next task was to find suitable analytical approximations for B_{sx}, B_{sy}, B_{sz}. It helps here to use coordinates tailored to the geometry of the current layer. Since the current is confined between the surfaces of constant $\xi_2 = \pm\Delta\xi_2$, it is natural to use the variable $t = \xi_2/\Delta\xi_2$ to define the position of a point in the direction transverse to the sheet, so that $-1 \le t \le +1$. On a surface of fixed t, two coordinates can define the position of a point. For one of them we chose $s = \cos\theta$, which was found to be approximately proportional to the distance L from the equatorial plane, measured along the stretched field line in units of the equatorial radius R_0 of that line. For the other coordinate, the solar-magnetic longitude ϕ was chosen. The coordinates $\{t, s, \phi\}$ are not orthogonal, but it does not matter for our purposes.

The components of the magnetic field within the current sheet were approximated and fitted by least squares, using the following functional forms:

$$B_x = \sum_{k=0}^{3}\sum_{l=1}^{5}\sum_{m=0}^{3} a_x^{(klm)} Q_k(t) S_l(s) \cos m\phi$$

$$B_y = \sum_{k=0}^{3}\sum_{l=1}^{5}\sum_{m=1}^{4} a_y^{(klm)} Q_k(t) S_l(s) \sin m\phi \qquad (21)$$

$$B_z = \sum_{k=0}^{3}\sum_{l=1}^{5}\sum_{m=0}^{3} a_z^{(klm)} Q_k(t) C_l(s) \cos m\phi$$

Each expansion contains 80 coefficients, found by least squares along with the nonlinear parameters entering in the factors $Q_k(t)$, $S_l(s)$, and $C_l(s)$. These are simple analytical functions, representing fundamental modes in the variation of the field components in the t and s directions. More specifically,

$$Q_0 = 1, \quad Q_1 = t(t^2 + t_0^2)^{-1/2},$$
$$Q_2 = t_0 Q_1', \quad Q_3 = -\left(\frac{2}{3}\right)\left(\frac{5}{4}\right)^{5/2} t_0 Q_2' \qquad (22)$$

and

$$S_l(s) = \begin{cases} \sqrt{-2eb_l}\, s \exp(b_l s^2) & \text{for } b_l < 0 \\ s \exp\left[b_l(s^2 - 1)\right] & \text{for } b_l \ge 0 \end{cases} \qquad (23)$$

$$C_l(s) = \begin{cases} \exp(b_l s^2) & \text{for } b_l < 0 \\ \exp\left[b_l(s^2 - 1)\right] & \text{for } b_l \ge 0 \end{cases} \qquad (24)$$

Figure 7 shows families of plots of the functions $Q_0 - Q_3$, S_l, and C_l, illustrating their behavior for different values of the parameters. Again, these functions are not orthogonal, in contrast to Chebyshev's polynomials, which were initially explored for that purpose. However, fitting by least squares does not require orthogonality of the modes; in addition, the above functions $Q_0 - Q_3$ tend to zero outside the current sheet, while the Chebyshev's polynomials rapidly diverge there, creating problems in splicing the approximation (17) to the outer and inner region solutions, as is discussed below in more detail.

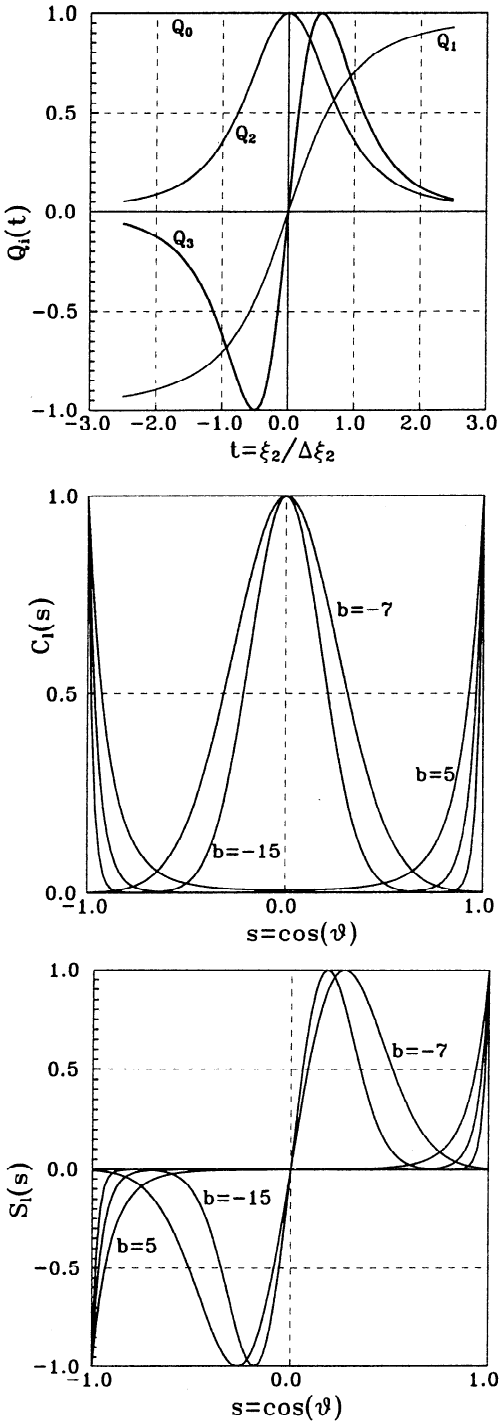

Figure 7. The functions $Q_0(t) - Q_3(t)$, $S_l(s)$, and $C_l(s)$, used as the fundamental modes in the expansions (21) approximating the field components inside the region 2 current sheet.

Fitting the expansions (21) to the Biot-Savart sets of values of B_x, B_y, and B_z provided the rms accuracies 3.1%, 1.9%, and 1.7%, respectively.

3.2.2. Matching the approximations at the current sheet boundaries. Since we approximate the field by different expansions in the three adjacent regions, it is important for the solutions to be smoothly joined at the boundaries in order to avoid abrupt jumps in the field components. That was handled by interpolating $\vec{\mathbf{B}}$ across strips centered on the boundaries. In the strips, the solutions from both sides were combined by means of a smooth weight function of the coordinate ξ_2, providing a gradual transition across the boundaries $\xi = -\Delta\xi_2$ and $\xi = +\Delta\xi_2$.

3.3. The Shielding Field for the Region 2 System

The shielding field for the region 2 current system was represented by combinations of the same set of potential fields as with region 1 currents, that is, by rectangular harmonics (13), and it was derived by the same method. In this case the sources of the field to be shielded lie entirely within the magnetosphere, and therefore their normal component on the magnetopause varied more smoothly, which is why the same set of rectangular harmonics yielded better accuracy (about 0.1%) than in the case of the region 1 currents.

4. Results

The main purpose of the preceding sections was to describe the methods that allowed us to develop a reasonable and relatively compact analytical representations for the large-scale systems of Birkeland currents. In this section, some results of testing the newly devised models for the region 1 and 2 field will be discussed. It should be kept in mind that the eventual goal of this study is to incorporate the Birkeland field models in a global data-based representation of the magnetospheric field and calibrate the intensity of region 1 and 2 systems as functions of the solar wind parameters and geophysical indices. Although the first results of such studies [*Tsyganenko and Stern*, 1995] have confirmed the feasibility of this approach, we relegate a detailed treatment of that subject for a separate paper.

Figure 8a shows the plots of the variation of the B_x component of the net disturbance field produced by the model Birkeland current systems, as would be seen by a spacecraft with a dawn-dusk circular orbit at an altitude of $H \approx 800$ km, similar to that of TRIAD or Magsat. The net currents in the region 1 and 2 systems were set equal to 2 MA and 1 MA, respectively, which roughly corresponds to the values reported by *Iijima and Potemra* [1976]. The profile is qualitatively similar to the typically observed variation of B_x [e.g., *Zanetti et al.*, 1983]: a nearly constant sunward field above the polar cap, rapid excursions of B_x on crossing the field-aligned current layers, and a relatively weak disturbance field at lower latitudes. Figure 8b shows the profile of numerically computed field-aligned current density, with the larger peaks from the region 1 system and smaller ones with the opposite polarity from the region 2 currents.

Figure 9 displays the distribution of the B_z component along the X_{GSM} axis, produced by the net region 1–2 system both on the dayside and on the nightside, and in Figure 10

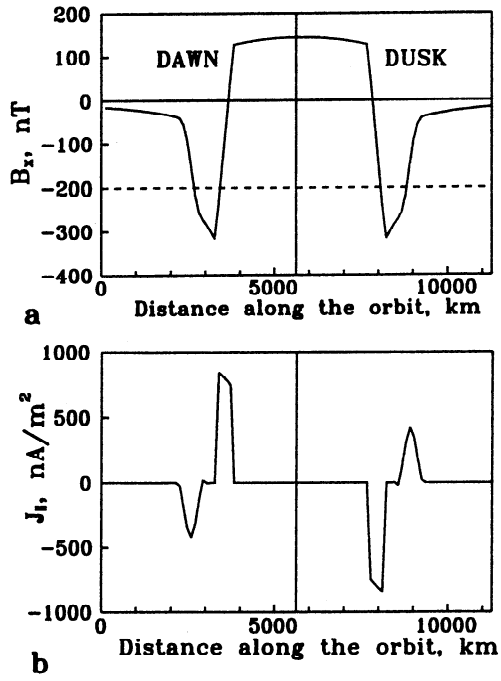

Figure 8. The dawn-dusk variation of (a) the B_x component of the magnetic field due to the region 1 and 2 current systems, as it would be measured by a low-altitude polar-orbiting spacecraft, and (b) the corresponding field-aligned component of the volume current density. The total magnitudes of the region 1 and 2 currents were set equal to 2 MA and 1 MA, respectively, in this example.

the corresponding nightside profile of the azimuthal component of the electric current is given (the equatorial current on the dayside is close to zero, since we assumed that all of the region 2 current closes on the nightside). The overall effect in B_z on the dayside is a negative disturbance that decreases with growing r, with $\Delta B \approx -10nT$ near the subsolar point. This result is close to the estimate by *Tsyganenko and Sibeck* [1994], for approximately the same values of the total current as in the present model. On the nightside, the negative

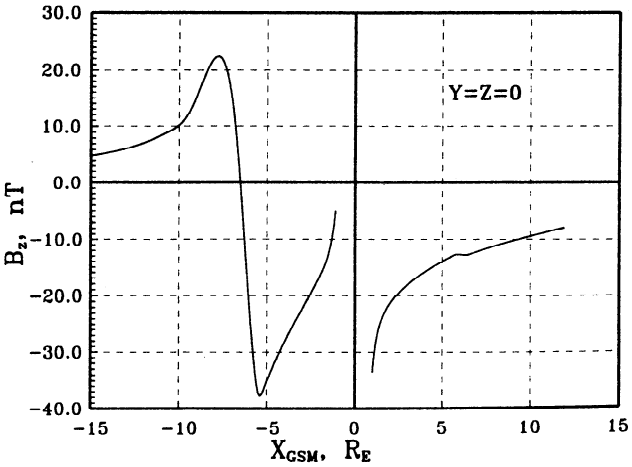

Figure 9. The profile of the magnetic field disturbance along the Sun-Earth line due to the region 1 and 2 current systems. The same magnitudes of the total currents, as in Figure 8, were assumed.

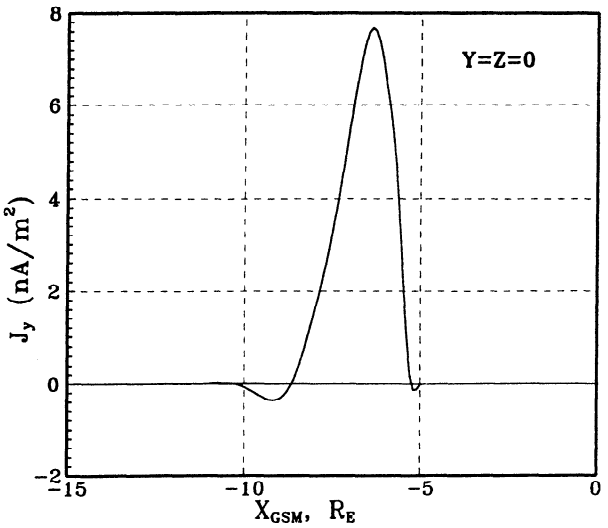

Figure 10. The nightside profile of the westward partial ring current density along the Sun-Earth line. The regions of small negative current at the edges are due to residual inaccuracy of the analytical approximation.

disturbance field increases outward, reaches the minimum of $\approx -40nT$ at $X_{GSM} \approx -5.5R_E$, makes a large excursion to positive values on crossing the partial ring current distributed within $r \sim 5-9R_E$, and gradually decays tailward. The corresponding electric current density, as expected, is smoothly distributed over a relatively large range of distances, as specified by the initial profile (14) assumed in the Biot-Savart calculations. Inaccuracies of the fitting expansions (21) give rise to unphysical oscillatory features near the boundaries of the partial ring current. However, their amplitudes are relatively small with respect to strong westward azimuthal currents due to the symmetrical ring current and the tail current sheet (not shown here), so that no major distortions of the magnetic configuration should be expected.

5. Summary

In this work we devised quantitative analytical models for the large-scale systems of Birkeland currents. The geometry of electric current flow lines and spatial distribution of the current density were specified by using Euler potentials, in agreement with existing data and physical constraints. The model's region of validity extends from ionospheric altitudes to the distant magnetosphere. The model includes a dependence of the current flow geometry on the Earth's dipole tilt and provides a smooth, spread-out distribution of the electric currents and magnetic field. The model is intended for inclusion in a global data-based quantitative representation of the external magnetospheric field, parametrized by the observed parameters of the solar wind and geophysical activity indices.

Acknowledgments. This work is supported by NASA grant NAS5-32350 and NSF Magnetospheric Physics Program grant ATM-9501463.

The Editor thanks G.-H. Voigt and another referee for their assistance in evaluating this paper.

References

Bythrow, P.F., and T.A. Potemra, The relationship of total Birkeland currents to the merging electric field, *Geophys. Res. Lett., 10,* 573–576, 1983.

Candidi, M., S. Orsini, M. Stokholm, and R. Elphic, On the structure of the tail magnetic field, *J. Geophys. Res., 95,* 7929–7936, 1990.

Donovan, E.F., Modeling the magnetic effects of field-aligned currents, *J. Geophys. Res., 98,* 13,529–13,543, 1993.

Hedgecock, P.C., and B.T. Thomas, HEOS observations of the configuration of the magnetosphere, *Geophys. J. R. Astron. Soc., 41,* 391–403, 1975.

Iijima, T., and T.A. Potemra, The amplitude distribution of field-aligned currents at northern high latitudes observed by Triad, *J. Geophys. Res., 81,* 2165–2174, 1976.

Janhunen, P., H.E.J. Koskinen, and T.I. Pulkkinen, A new global ionosphere-magnetosphere coupling simulation utilizing locally varying time step, in *3rd International Conference on Substorms,* Versailles, France, May 12–17, 1996, in press, 1996.

Mead, G.D., and D.H. Fairfield, A quantitative magnetospheric model derived from spacecraft magnetometer data, *J. Geophys. Res., 80,* 523–534, 1975.

Schulz, M., and M. McNab, Source-surface model of the magnetosphere, *Geophys. Res. Lett., 14,* 182–185, 1987.

Sotirelis, T., N.A. Tsyganenko, and D.P. Stern, A method for confining the magnetic field of the cross-tail current inside the magnetosphere, *J. Geophys. Res., 99,* 19,393–19,402, 1994.

Stern, D.P., The origin of Birkeland currents, *Rev. Geophys., 21,* 125–138, 1983.

Stern, D.P., Tail modeling in a stretched magnetosphere, 1. Methods and transformations, *J. Geophys. Res., 92,* 4437–4448, 1987.

Stern, D.P., A simple model of Birkeland currents, *J. Geophys. Res., 98,* 5691–5706, 1993.

Tanaka, T., Generation mechanisms for magnetosphere-ionosphere current systems deduced from a three-dimensional MHD simulation of the solar wind-magnetosphere-ionosphere coupling processes, *J. Geophys. Res., 100,* 12,057–12,076, 1995.

Toffoletto, F.R., and T.W. Hill, Mapping of the solar wind electric field to the Earth's polar caps, *J. Geophys. Res., 94,* 329–347, 1989.

Troshichev, O.A., Polar magnetic disturbances and field-aligned currents, *Space Sci.Rev., 32,* 275–354, 1982.

Tsyganenko, N.A., Global quantitative models of the geomagnetic field in the cislunar magnetosphere for different disturbance levels, *Planet. Space Sci., 35,* 1347–1358, 1987.

Tsyganenko, N.A., Quantitative model of the system of field-aligned magnetospheric currents, *Geomagn. Aeron.*, Engl. Transl., *28,* 331–335, 1988.

Tsyganenko, N.A., A magnetospheric magnetic field model with a warped tail current sheet, *Planet. Space Sci., 37,* 5–20, 1989.

Tsyganenko, N.A., Methods for quantitative modeling of the magnetic field from Birkeland currents, *Planet. Space Sci., 39,* 641–654, 1991.

Tsyganenko, N.A., A global analytical representation of the magnetic field produced by the region 2 Birkeland currents and the partial ring current, *J. Geophys. Res., 98,* 5677–5690, 1993.

Tsyganenko, N.A., Modeling the Earth's magnetospheric magnetic field confined within a realistic magnetopause, *J. Geophys. Res., 100,* 5599–5612, 1995.

Tsyganenko, N.A., and D.G. Sibeck, Concerning flux erosion from the dayside magnetosphere, *J. Geophys. Res., 99,* 13,425–13,436, 1994.

Tsyganenko, N.A. and D.P. Stern, Birkeland currents in the data-based magnetospheric field models (abstract) *Eos Trans. AGU, 76*(46), Fall Meet. Suppl., 497, 1995.

Tsyganenko, N.A., D.P. Stern, and Z. Kaymaz, Birkeland currents in the plasma sheet, *J. Geophys. Res., 98,* 19,455–19,469, 1993.

Zanetti, L.J., W. Baumjohann, and T.A. Potemra, Ionospheric and Birkeland current distributions inferred from the Magsat magnetometer data, *J. Geophys. Res., 88,* 4875–4884, 1983.

Zmuda, A.J. and J.C. Armstrong, The diurnal flow pattern of field-aligned currents, *J. Geophys. Res., 79,* 4611–4619, 1974.

D. P. Stern, Laboratory for Extraterrestrial Physics, Code 695, NASA Goddard Space Flight Center, Greenbelt, MD 20771. (e-mail: u5dps@lepvax.gsfc.nasa.gov)

N. A. Tsyganenko, Hughes STX Corporation, Laboratory for Extraterrestrial Physics, Code 695, NASA Goddard Space Flight Center, Greenbelt, MD 20771. (e-mail: ys2nt@lepvax.gsfc.nasa.gov)

(Received April 9, 1996; revised July 19, 1996;
accepted September 4, 1996.)